Scheme and application of phase delay spectrum towards spatial stochastic wind fields

Qi Yan[1], Yongbo Peng[2,3] and Jie Li [*1,2]

[1]*School of Civil Engineering, Tongji University, Shanghai 200092, China*
[2]*State Key Laboratory of Disaster Reduction in Civil Engineering, Tongji University, China*
[3]*Shanghai Institute of Disaster Prevention and Relief, Tongji University, China*

Abstract. A phase delay spectrum model towards the representation of spatial coherence of stochastic wind fields is proposed. Different from the classical coherence functions used in the spectral representation methods, the model is derived from the comprehensive description of coherence of fluctuating wind speeds and from the thorough analysis of physical accounts of random factors affecting phase delay, building up a consistent mapping between the simulated fluctuating wind speeds and the basic random variables. It thus includes complete probabilistic information of spatial stochastic wind fields. This treatment prompts a ready and succinct scheme for the simulation of fluctuating wind speeds, and provides a new perspective to the accurate assessment of dynamic reliability of wind-induced structures. Numerical investigations and comparative studies indicate that the developed model is of rationality and of applicability which matches well with the measured data at spatial points of wind fields, whereby the phase spectra at defined datum mark and objective point are feasibly obtained using the numerical scheme associated with the starting-time of phase evolution. In conjunction with the stochastic Fourier amplitude spectrum that we developed previously, the time history of fluctuating wind speeds at any spatial points of wind fields can be readily simulated.

Keywords: phase delay spectrum; stochastic wind field; spatial coherence; coherence function; wind field simulation; spectral representation method

1. Introduction

The coherence properties of wind fields refer to the statistical relationship between time histories of wind speeds of any two spatial points in frequency domain, which is usually denoted as a coherence function. Panofsky and McCormick first presented the concept of Coherence for wind engineering in 1954 by revealing the conjunctive spectrum and orthometric spectrum of a cross-power spectrum of two segments of wind speed time series (Panofsky and McCormick 1954). The pioneered experimental investigation was carried out by A.G. Davenport, who proposed the celebrated exponential decaying model of coherence function for vertical and horizontal wind fields, respectively, according to the measured data (Davenport 1961, 1967). This model was then

---

∗Corresponding author, Professor, E-mail: lijie@tongji.edu.cn

proved by other researchers and has been widely used up to date (Panofsky and Singer 1965, Kristensen *et al.* 1981, Chen 1994, Ying *et al.* 2005, Paroka and Umeda 2006, Collins *et al.* 2008).

Although the exponential coherence model exhibits a feasible behavior to practical applications, a critical issue inherent in this model does exist. It is noted that the Davenport exponential model is always valued by 1 at the frequency zero, which does not match with the measured data in case that the two spatial points have a farther distance (Dyrbye and Hansen 1997). The model, moreover, may not be appropriate especially for modeling the coherence of the vertical turbulence component since it fails to account for reductions in coherence at low frequencies and over large separations (Saranyasoontorn *et al.* 2004). In conjunction with von Karman theory, Harris derived a coherence function of fluctuating wind speeds of two spatial points at isotropic turbulence fields (Harris 1971), which is the well-known Harris model in wind engineering. The Harris model, noted by Maeda and his colleagues, is suitable for describing the coherent behaviors of measured fluctuating wind speeds, while it is not feasible for engineering applications due to a family of complicated Bessel functions involved in the model. A simplified formula based on the Harris model was then proposed (Maeda and Makino 1980). It was found, however, that at large separations the turbulent wind field is not isotropic, and the isotropic von Karman model to describe the coherence function for such distances is not available (Schlez and Infield 1998). Another exponential coherence model accounting for the influence of turbulence intensity and the angular dependence of horizontal coherence was proposed (Schlez and Infield 1998).

The coherence function is viewed as the most important argument representing the mathematical and physical structures of spatial wind fields. It serves as a critical component in the simulation of wind fields whether using the classical spectral representation method or using the linear filtering scheme (Shinozuka and Jan 1972). While the coherence function is essentially the statistical characteristics whereby the simulated random process does not include the probabilistic information with statistical moments more than second order.

It is found in our investigations that the differences between two Fourier phase spectra indicates the similarities of corresponding time histories of wind speeds at any two spatial points, and govern their coherence behaviors as well. A phase delay spectrum model is thus developed in the present paper that describes the spatial coherence of stochastic wind fields and accommodates the simulation of large-scale wind fields. The rationality and of applicability of the model is proved using the measured data at spatial points of wind fields. The sections arranged in this paper are distributed as follows. Section 2 is dedicated to illustrating the relationship between phase delay spectrum and coherence function. The modeling and validation of phase delay spectrum, including those along vertical and horizontal directions, are respectively provided in Section 3. Section 4 details the numerical procedure of simulation of multiple-point fluctuating wind speeds. Discussion on the spectral representation method and the proposed simulation scheme is carried out in Section 5. The concluding remarks are included in the final section.

2. Relationship between phase delay spectrum and coherence function

2.1 Definition of coherence function and its numerical scheme

The coherence function γ_u between the two fluctuating wind speeds u_x and u_y at any two spatial points along the main direction of wind field can be defined as

$$\gamma_u(n) = \frac{\left|S_{xy}(n)\right|}{\sqrt{S_{xx}(n)}\sqrt{S_{yy}(n)}}$$

(1)

Where S_{xy} denotes the cross-spectral density of u_x and u_y; S_{xx} and S_{yy} denotes the auto-spectral density of u_x and u_y, respectively; n denotes the natural frequency.

The numerical scheme of spectral density of fluctuating wind speeds using periodogram technique is detailed as follows (Welch 1967)

The fluctuating wind speeds u_x and u_y are assumed as the ensemble of N samples of time histories $u_{x_1}, \cdots, u_{x_N}$ and $u_{y_1}, \cdots, u_{y_N}$, respectively. The sampling number in each section is D, and the sampling frequency denotes F_s. The time duration of each sample denotes $T = D/F_s$. The discrete Fourier transform (DFT) of each sample of u_x and u_y is carried out employing the following formula

$$F_{x_j}(n) = \frac{1}{\sqrt{T}}\sum_{k=1}^{D}u_{x_j}(k/F_s)\exp[-\mathrm{i}2\pi(k-1)(nT-1)]\Delta t, \quad j = 1, 2, ..., N$$

(2)

$$F_{y_j}(n) = \frac{1}{\sqrt{T}}\sum_{k=1}^{D}u_{y_j}(k/F_s)\exp[-\mathrm{i}2\pi(k-1)(nT-1)]\Delta t, \quad j = 1, 2, ..., N$$

(3)

where i denotes the unit length of imaginary number $\sqrt{-1}$.

The auto-spectral density of the fluctuating wind speeds u_x and u_y is rendered by

$$S_{xx}(n) = E[F_{x_j}(n)F_{x_j}^*(n)] = \sum_{j=1}^{N}\frac{1}{N}F_{x_j}(n)F_{x_j}^*(n)$$
$$= \sum_{j=1}^{N}\frac{1}{N}\left|F_{x_j}(n)\right|^2 = E[\left|F_{x_j}(n)\right|^2]$$

(4)

$$S_{yy}(n) = E[F_{y_j}(n)F_{y_j}^*(n)] = \sum_{j=1}^{N}\frac{1}{N}F_{y_j}(n)F_{y_j}^*(n)$$
$$= \sum_{j=1}^{N}\frac{1}{N}\left|F_{y_j}(n)\right|^2 = E[\left|F_{y_j}(n)\right|^2]$$

(5)

where the superscript '*' denotes the conjugation of complex number; $E[\cdot]$ denotes the ensemble-average of argument.

The cross-spectral density of the fluctuating wind speeds u_x and u_y is rendered by

$$S_{xy}(n) = E[F_{x_j}(n)F_{y_j}^*(n)] = \sum_{j=1}^{N} \frac{1}{N} F_{x_j}(n)F_{y_j}^*(n) = E[F_{x_j}(n)F_{y_j}^*(n)]$$

(6)

Substitution of Eqs. (4), (5) and (6) into Eq. (1), the coherence function can then be derived

$$\gamma_u(n) = \frac{\left| E[F_{x_j}(n)F_{y_j}^*(n)] \right|}{\sqrt{E[\left|F_{x_j}(n)\right|^2]}\sqrt{E[\left|F_{x_j}(n)\right|^2]}}$$

(7)

2.2 Relationship between coherence function and Fourier spectrum

The discrete Fourier transform denoted by Eqs. (2) and (3) can be re-written into the function in Fourier amplitude and Fourier phase

$$F_{x_j}(n) = \left| F_{x_j}(n) \right| \exp[i\phi_{x_j}(n)]$$

(8)

$$F_{y_j}(n) = \left| F_{y_j}(n) \right| \exp[i\phi_{y_j}(n)]$$

(9)

where $\left| F_{x_j}(n) \right|$ and $\left| F_{y_j}(n) \right|$ denote the Fourier amplitude spectrum; $\phi_{x_j}(n)$ and $\phi_{y_j}(n)$ denote the Fourier phase spectrum.

The conjunctive spectrum of Fourier spectrum is given by

$$F_{x_j}^*(n) = \left| F_{x_j}(n) \right| \exp[-i\phi_{x_j}(n)]$$

(10)

$$F_{y_j}^*(n) = \left| F_{y_j}(n) \right| \exp[-i\phi_{y_j}(n)]$$

(11)

The cross-power spectrum denoted in Eq. (6) can be re-written into

$$S_{xy}(n) = E[F_{x_j}(n)F_{y_j}^*(n)] = E[\left| F_{x_j}(n) \right| \left| F_{y_j}(n) \right| \exp(i(\phi_{x_j}(n) - \phi_{y_j}(n)))]$$

(12)

The coherence function denoted in Eq. (7) then can be re-written into

$$\gamma_u(n) = \frac{\left| E[\left| F_{x_j}(n) \right| \left| F_{y_j}(n) \right| \exp(i\Delta\phi_j(n))] \right|}{\sqrt{E[\left|F_{x_j}(n)\right|^2]}\sqrt{E[\left|F_{y_j}(n)\right|^2]}}$$

(13)

where $\Delta\phi_j(n)$ denotes the phase delay spectrum of two spatial points at wind field

$$\Delta\phi_j(n) = \phi_{x_j}(n) - \phi_{y_j}(n)$$

(14)

Assuming $\left|F_{x_j}(n)\right|$, $\left|F_{y_j}(n)\right|$ and $\Delta\phi_j(n)$ are mutually independent stochastic variables at the points of frequencies, we then have

$$\left|E[\left|F_{x_j}(n)\right|\left|F_{y_j}(n)\right|\exp(i\Delta\phi_j(n))]\right| = \left|E[\left|F_{x_j}(n)\right|]\right| \cdot \left|E[\left|F_{y_j}(n)\right|]\right| \cdot \left|E[\exp(i\Delta\phi_j(n))]\right|$$

(15)

While there has

$$E\left[\left|F_{x_j}(n)\right|^2\right] = \left(E\left[\left|F_{x_j}(n)\right|\right]\right)^2 + \left(D\left[\left|F_{x_j}(n)\right|\right]\right)^2$$

(16)

Eq. (13) is then reduced into

$$\gamma_u(n) = \frac{\left|E\left[\exp(i\Delta\phi_j(n))\right]\right|}{\sqrt{1 + \frac{\left(D\left[\left|F_{x_j}(n)\right|\right]\right)^2}{\left(E\left[\left|F_{x_j}(n)\right|\right]\right)^2}}\sqrt{1 + \frac{\left(D\left[\left|F_{y_j}(n)\right|\right]\right)^2}{\left(E\left[\left|F_{y_j}(n)\right|\right]\right)^2}}}$$

(17)

where $D[\cdot]$ denotes the standard deviation of argument.

It is indicated in the Fourier amplitude spectrum of measured fluctuating wind speeds that its standard deviation is 10%-30% of the mean (Li *et al.* 2012). One might figure out that the denominator in Eq. (17) values 1.01-1.09. Eq. (17) then can be further reduced into

$$\gamma_u(n) = \left|E\left[\exp(i\Delta\phi_j(n))\right]\right| = \left|E\left[\cos(\Delta\phi_j(n)) + i\sin(\Delta\phi_j(n))\right]\right|$$

(18)

The reducing formulation of coherence function $\gamma_u(n)$ is built up on the error less than 10%.

It is revealed by Eq. (18) that the coherence function relies upon the phase delay spectrum that indicates the critical factor governing the difference and relationship between time histories of fluctuating wind speeds at any two spatial points of wind fields.

One might realize that the phase delay spectrum of Fourier spectrum is a stochastic variable due to the randomness inherent with the spatial wind fields. The general formulation of the phase

delay spectrum is given by $\Delta\phi(n,\eta;x_1,y_1,z_1,x_2,y_2,z_2)$, where η denotes the elementary stochastic variable; $(x_1,y_1,z_1,x_2,y_2,z_2)$ denotes the spatial variables of wind fields.

The phase spectrum $\phi_{y_j}(n)$ might be denoted as a coordinative phase spectrum if the spatial point y of wind field is defined as a coordinative point where the fluctuating wind speed u_y is measured. The phase spectrum of fluctuating wind speed $\phi_{x_j}(n)$, in this context, at any spatial point x can be derived using Eq. (14) in case that the phase delay spectrum $\Delta\phi_j(n)$ between spatial points x and y. In conjunction with the Fourier amplitude spectrum $\left|F_{x_j}(n)\right|$ of fluctuating wind speeds (Li *et al.* 2012), the fluctuating wind speed u_x at the spatial points x can be readily re-built up by virtue of Eq. (10) and its inverse Fourier transform. Using this numerical scheme, the spatial wind field can be constructed.

Since the Fourier amplitude spectrum and Fourier phase spectrum of fluctuating wind speeds both be expressed in stochastic functions, the mentioned numerical scheme, based on the principle 'coordinative phase spectrum—phase delay spectrum', is rendered to implement the simulation of spatial stochastic wind fields.

The phase values of phase delay spectrum $\Delta\phi(n)$ typically locate at the domain $[0,\infty]$, while its principal values are usually defined in the domain $[0,2\pi]$. Fig. 1 shows the principal value $\Delta\phi_{xy}(n)$ of the two cases with relative relationship between $\phi_x(n)$ and $\phi_y(n)$. It is indicated that any phase delay spectrum can be transferred into its counterpart with principal values using the complementation scheme by 2π.

It is noted that the stochastic model of wind fields using phase delay spectrum and that of wind fields using coherence function have some connections as well as differentiation. The coherence function, as indicated in Eq. (18), can be derived from the phase delay spectrum by operating its argument in harmonic functions with mathematic expectation. While the two components have significant differences from the sample collection that would be detailed in the following sections.

3. Modeling of phase delay spectrum

3.1 Primary factors affecting phase delay spectrum

The previous investigations indicate that the main factor affecting the wave shape of a time history of wind velocity is its Fourier phase spectrum (Seong and Peterka 2001). Although the Fourier amplitude spectrum hinges on the energy distribution of wind velocity process, it does not govern the wave shape. In fact, the wave shape exhibits a certain similarity between wind speed time series recorded at two spatial points in the neighborhood. The closer of the two points, the more obvious of similarity of wave shape arises to be and vice versa. It is thus remarked that the degree of similarity of Fourier phase spectrum of wind speeds recorded at two closer spatial points is higher than that of wind speeds recorded at two distant spatial points. In other words, the phase delay spectrum defined in Eq. (14) would be of a smaller value as far as the wind speeds recorded at a two closer spatial points are concerned.
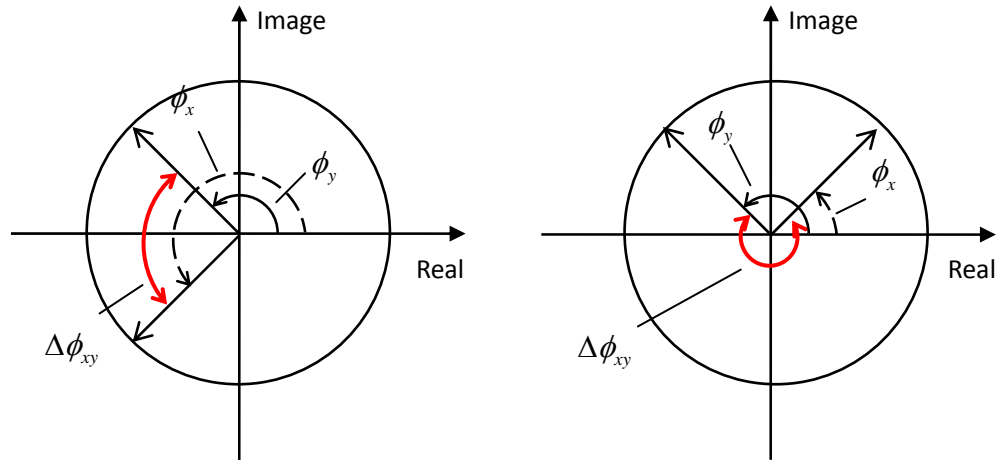
Fig. 1 Indication of principal values of phase delay spectrum

The investigations reveal that the primary factors affecting the phase delay spectrum include: (i) the natural frequency n that is in positive relationship to the phase delay; (ii) the spatial distance r_y and r_z between two points that are also in positive relationship to the phase delay; (iii) the mean wind speed $\overline{U}$ that is in negative relationship to the phase delay; (iv) the shear rate $d\overline{U}/dz$ that is in positive relationship to the phase delay. The decaying exponential model of coherence function includes the first three factors but not includes the fourth factor. As a matter of fact, the influence of surface friction on the airflow at high altitude can be ignored, and the airflow gives rise to be isotropic turbulence. This influence, however, appears to be strong in the domain near the surface. The direct proof is that the difference between wave shape of wind speed time series at two low-altitude spatial points exhibits to be more significant than that at two high-altitude spatial points. The shear rate of main flow, therefore, should be accounted into the phase delay spectrum. The model of phase delay spectrum developed in the present paper includes the influence of the shear rate.

3.2 Model of phase delay spectrum

The mentioned four factors affecting phase delay should be included in the model of phase delay spectrum. While the model could be represented by these factors through dimensional analysis since the phase delay is really a dimensionless quantity. According to the relationship between the phase delay spectrum and these four factors, the mean wind speed is supposed to be an argument serving as the denominator, while the other three factors are supposed to be arguments serving as the numerator. Having this in mind, we propose the model of phase delay spectrum as follows

$$\Delta\phi_y(n) = \frac{\beta_y r_y \left(n \dfrac{d\overline{U}}{dz} \right)^{0.5}}{\overline{U}}$$

(19)

$$\Delta\phi_z(n) = \frac{\beta_z r_z \left(n \dfrac{d\overline{U}}{dz} \right)^{0.5}}{\overline{U}}$$

(20)

where β_y and β_z denote the magnification coefficient of phase delay spectrum along horizontal direction and vertical direction, respectively, whereby the phase delay spectrum with different amplitudes can be obtained.

Eqs. (19) and (20) represent a collection of phase delay spectra, respectively. The phase delay spectrum, moreover, is essentially a stochastic function of which the basic stochastic variables are the mean wind speed $\overline{U}$ and the ground roughness length z_0. It is understood from the log-law formulation of wind profile

$$\overline{U}(z) = \frac{u_*}{\kappa} \ln \frac{z}{z_0}$$

(21)

where u_* denotes the shear wave speed; κ denotes the von Karman's constant. Differential of Eq. (21) with respect to height z, the shear rate of main flow in the time domain can be obtained

$$\frac{d\overline{U}(z)}{dz} = \frac{u_*}{\kappa z}$$

(22)

It was mentioned previously that the phase delay spectrum is a stochastic function in essence. When using Eqs. (19) and (20) in usual cases, the mean wind speed $\overline{U}$ and shear rate $d\overline{U}(z)/dz$ are typically valued by their means.

3.3 Validation of phase delay spectrum along vertical direction

It is indicated that there exists the relationship of samples and set between Fourier amplitude spectrum and the power spectrum (Li *et al*. 2012). The power spectrum can be derived from the integration of samples of Fourier amplitude spectrum. Likewise, there exists the relationship of samples and set between phase delay spectrum and the coherence function, as shown in Eq. (13), where the ensemble-average of the function dependent upon phase delay spectrum results in an approximate coherence function. It is thus necessary to carry out the validation of phase delay spectrum.

The formulation of coherence function is given by

$$\gamma_u(z_0, \overline{U}_{ref}, n) = \left| E[\exp(\mathrm{i}\Delta\phi_j(n))] \right| = \left| \iint\limits_{\Omega} [\cos(\Delta\phi_j(n)) + \mathrm{i}\sin(\Delta\phi_j(n))] p(\overline{U}_{ref}) p(z_0) d\overline{U}_{ref} dz_0 \right|$$
(23)

where $p(\overline{U}_{ref})$ and $p(z_0)$ denote the probability density functions of mean wind speed at the reference height and of the ground roughness length, respectively. Ω denotes the integral domain.

As far as the phase delay spectrum along vertical direction is concerned, the mean wind speed $\overline{U}(z)$ at height z relies upon the ground roughness length and the mean wind speed at the reference height z_{ref}

$$\overline{U}(z) = \frac{\overline{U}(z_{ref})\ln(z/z_0)}{\ln(z_{ref}/z_0)}$$
(24)

then the shear rate is given by

$$\frac{d\overline{U}(z)}{dz} = \frac{\overline{U}(z_{ref})}{z\ln(z_{ref}/z_0)}$$
(25)

The ground roughness length z_0 is assumed to admit the log-normal distribution. The reference height is defined as 10 m. The mean wind speed $\overline{U}_{10}$ is assumed to admit Gumbel distribution (Li *et al.* 2012). Towards obtaining the measured data of strong winds, we built up an observation platform at a certain site of East China in 2006. The surroundings of the platform are schematically plotted in Fig. 2. A main anemometer tower, denoted as P1 shown in Fig. 3, is used as the primary carrier for investigating the vertical wind field. Other three anemometer towers, denoted as P2, P3, P4, respectively, in Fig. 3, were also erected in the area of platform to investigate the horizontal wind field. Four supersonic anemometers were mounted on the main tower, as shown in Fig. 3, at 10 m; 20 m; 28 m and 43 m along the height of the anemometer tower, respectively. The wind data was measured using these supersonic anemometers of which the sample frequency is 10 Hz. Huge mass of wind-speed data has been obtained in the past 5 years. The profile of mean wind speeds can be obtained through synthesizing the measured data of wind speeds into the time interval 10 mins at these typical heights. Fig. 4 shows the profile of a 10-min mean wind speed from measured data and its fitting function, respectively. It is seen that the wind profile match well with the log-law formulation, as indicated in Eq. (21). The turbulence intensity along the main flow, defined as the ratio between standard of deviation of fluctuating wind speeds and the mean wind speed, at height 10 m is identified to be 0.25 using the measured data. The statistical parameters of the ground roughness length z_0 and the mean wind speed $\overline{U}_{10}$ are listed in Table 1.
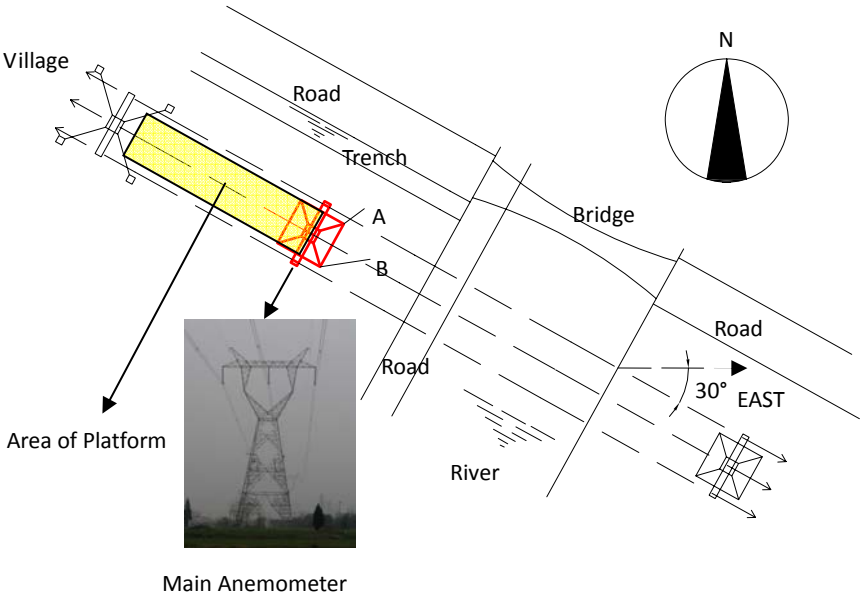
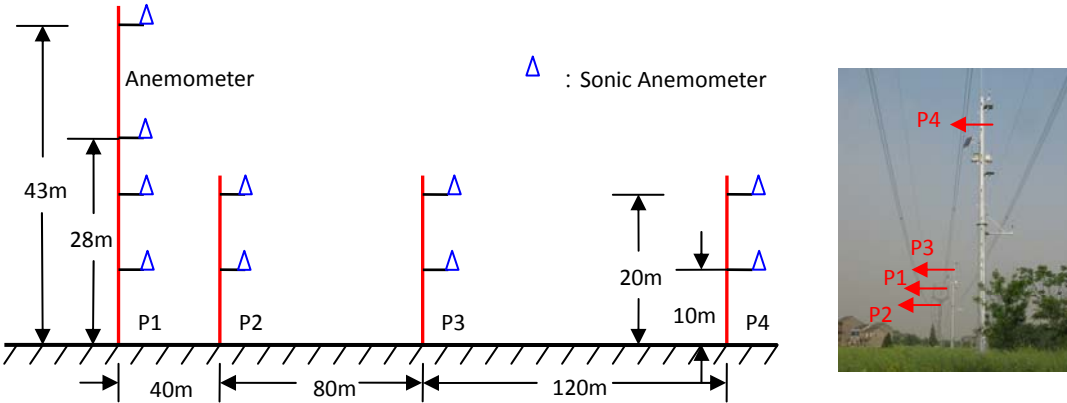Fig. 2 Schematic diagram of surroundings of the platform

Fig. 3 Schematic diagram of four supersonic anemometers mounted on the anemometer tower

Table 1 Statistical parameters relevant to probability density of elemental stochastic variables

Stochastic variables	z_0	$\overline{U}(z)$			
		10 m	20 m	28 m	43 m
Mean	-1.2155	--	--	--	--
Standard deviation	1.0052	--	--	--	--
Position parameter	--	5.1746	6.3349	6.7712	7.5151
Scale parameter	--	0.7475	0.8286	0.8402	1.0337
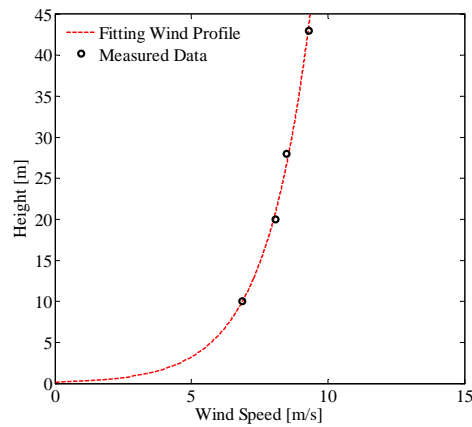
Fig. 4 Profile of a 10-min mean wind speed from measured data and its fitting function

We choose 20 sample values with equivalent probability respectively on the ground roughness length z_0 and the mean wind speed $\overline{U}_{10}$. For the purpose of comparative studies, the height 10 m is defined as the reference height. Three collections of phase delay spectra respectively at the height 20 m, 28 m and 43 m are generated using the proposed model. Each collection includes 400 samples. The coherence function derived from Eq. (23) is modified to match the coherence function derived from the measured data through adjusting the magnification coefficient of phase delay spectrum β_z, as shown in Fig. 5.
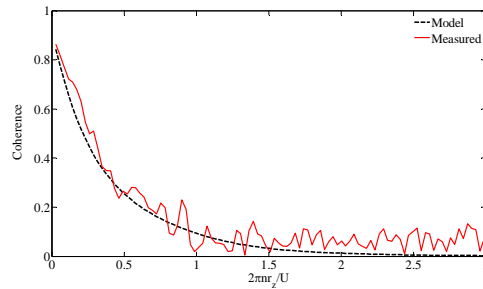
It was mentioned that Eq. (13) just indicates the ensemble-average of the phase delay spectrum in complex domain. While its standard deviation can be further defined by

$$\delta_u(n) = \left| D[\exp(\mathrm{i}\Delta\phi_j(n))] \right| = \left| \sqrt{\iint_\Omega (\cos\Delta\phi_j(n) - E[\cos\Delta\phi_j(n)])^2 \, p(\overline{U}_{10}) \, p(z_0) \, d\overline{U}_{10} \, dz_0} \right.$$

$$\left. + \mathrm{i}\sqrt{\iint_\Omega (\sin\Delta\phi_j(n) - E[\sin\Delta\phi_j(n)])^2 \, p(\overline{U}_{10}) \, p(z_0) \, d\overline{U}_{10} \, dz_0} \right| \tag{26}$$

The standard deviation of coherence functions along vertical direction derived from measured data and model is shown in Fig. 6.
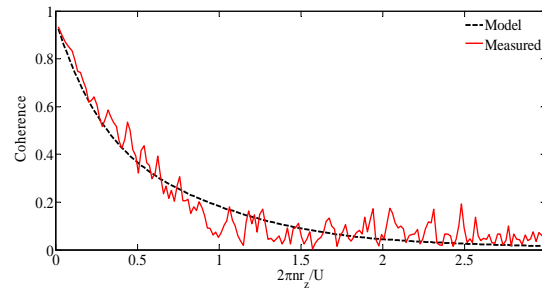
(a) $r_z = 10$ m (HT: 10 m and 20 m, $\beta_z = 80$)

(b) $r_z = 18$ m (HT: 10 m and 28 m, $\beta_z = 80$)

(c) $r_z = 33$m (HT: 10m and 43m, $\beta_z = 65$)

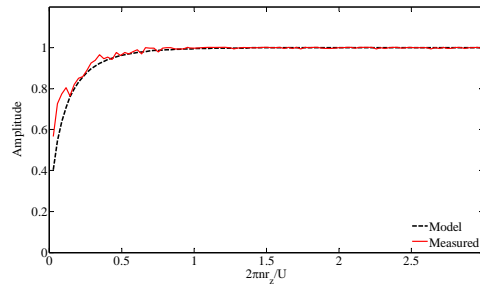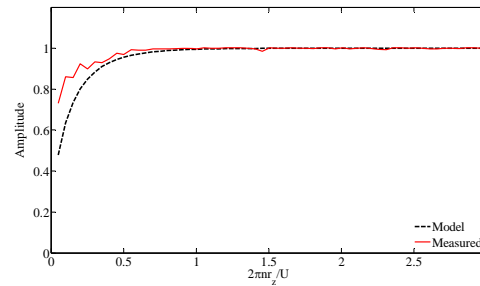Fig. 5 Mean of coherence functions along vertical direction derived from measured data and model

(a) r_z =10 m (HT: 10 m and 20 m, β_z =80)

(b) r_z =18 m (HT: 10 m and 28 m, β_z =80)

(c) r_z =33 m (HT: 10 m and 43 m, β_z =65)

Fig. 6 Standard deviation of coherence functions along vertical direction derived from measured data and model

It is seen that the standard deviation of coherence function derived from measured data is slightly larger than that of coherence function derived from the model in the domain of low frequencies, indicating that the measured phase delay features a wider distribution in the complex domain. Besides, the standard deviation whether of the measured spectrum or of the model spectrum approaches to 1. It is revealed that the principal values of phase delay spectrum admit the uniform distribution with domain of $[0, 2\pi)$.

3.4 Validation of phase delay spectrum along horizontal direction

   The cross-wind distance between two spatial points of wind field at horizontal direction is not always the direct distance between them, especially in case that the along-wind direction is not perpendicular to the direction connected by the two points, as shown in Fig. 7.

   It is worth to be noted that the phase delay spectrum described by Eq. (19) is between spatial points P and P_1. While the phase delay spectrum between spatial points P_1 and P_2 should account for the along-wind phase delay between P_2 and P, which is given by

$$\Delta\phi_x(n) = 2\pi \frac{r_x}{\overline{U}} n$$
(27)

   It is indicated in Eq. (27) that the along-wind phase delay derives from the product of 2π and the ratio between along-wind distance r_x and harmonic wave length $\overline{U}/n$. As regards the case shown in Fig. 7, therefore, Eq. (19) should be modified into

$$\Delta\phi_y(n) = \frac{\beta_y r_y \left(n\dfrac{d\overline{U}}{dz} \right)^{0.5}}{\overline{U}} + \frac{2\pi n r_x}{\overline{U}}$$
(28)

   It is obvious that the along-wind distance r_x would be zero in case that the along-wind direction is perpendicular to the direction connected by the two points, and Eq. (28) becomes into Eq. (19).
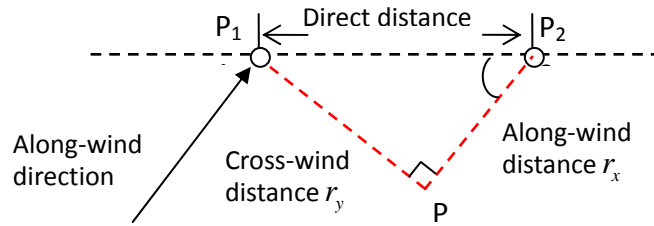

Fig. 7 Schematic diagram of relationship between cross-wind distance and direct distance between two spatial points P1 and P2

   We select 66-group measured data of wind speeds to calculate the coherence function and its standard deviation at which the wind direction almost exhibits 30 degree (± 5 degree) to the direction of wind-field platform. The model computation, meanwhile, are carried out using Eqs. (23) and (26). The reference height is defined as 20 m. Since the angle between along-wind direction and direction of wind-field platform is about 30 degree, the cross-wind distance is just half of the direct distance. Defining the point P_1 as the datum mark, the phase delay spectrum of
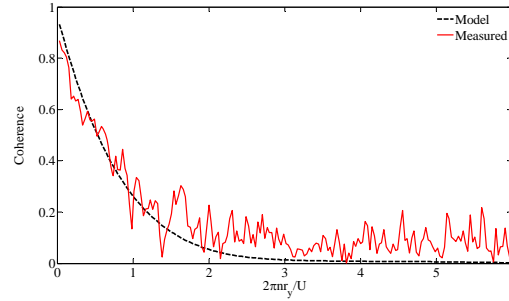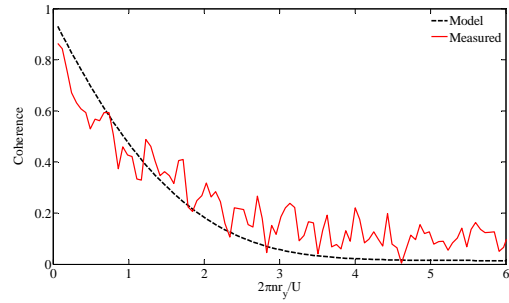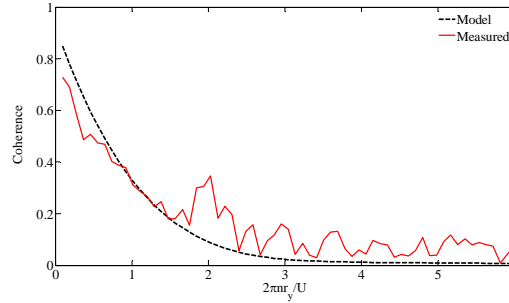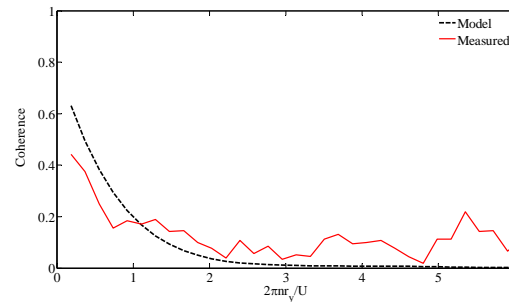
(a) r_y =20 m (PT: P$_1$ and P$_2$, β_y =60)

(b) r_y =40 m (PT: P$_2$ and P$_3$, β_y =30)

(c) r_y =60 m (PT: P$_1$ and P$_3$, β_y =30)

(d) r_y =120 m (PT: P$_1$ and P$_4$, β_y =25)

Fig. 8 Mean of coherence functions along horizontal direction derived from measured data and model

the wind speed at the neighborhood points with distance along cross-wind direction 20 m, 60 m and 120 m can be readily obtained, respectively. Besides, the phase delay spectrum with distance 40 m can also be derived defining P_2 as the datum mark and P_3 as the neighborhood point.

(a) r_y =20 m (PT: P_1 and P_2, β_y =60)

(b) r_y =40 m (PT: P_2 and P_3, β_y =30)

(c) r_y =60 m (PT: P_1 and P_3, β_y =30)

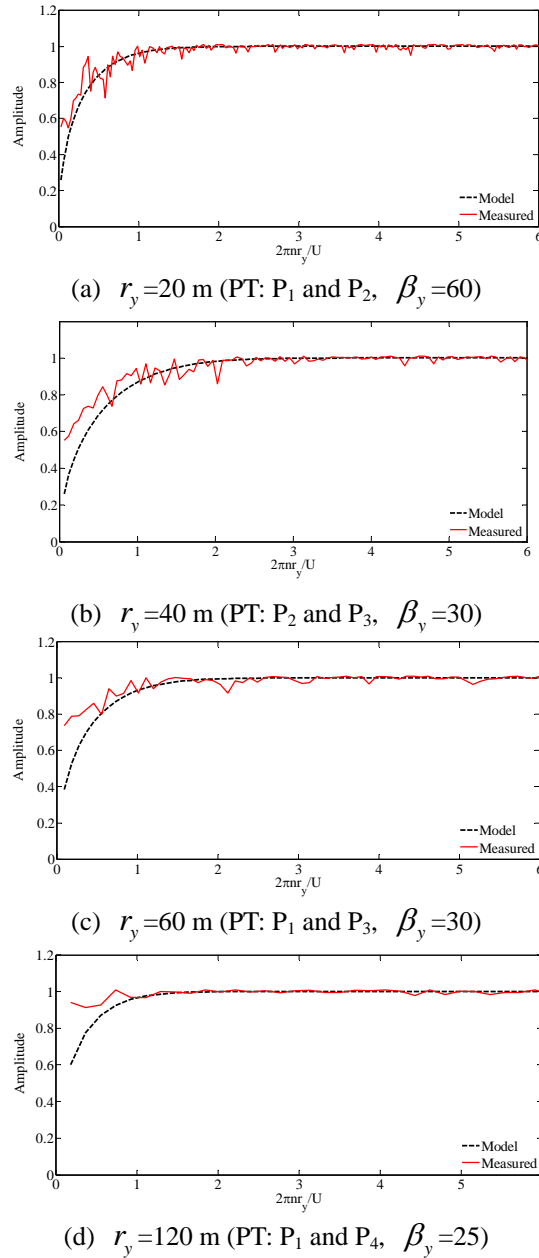(d) r_y =120 m (PT: P_1 and P_4, β_y =25)

Fig. 9 Standard deviation of coherence functions along horizontal direction derived from measured data and model

Figs. 8 and 9 show the defference between the results derived from model and from the measured data. It is seen that the coherence function computed by the proposed model of phase delay spectrum matches well with that computed by measured data. This is true whether for the mean or the standard deviation of phase delay spectrum. It is thus proved that the modified model represented by Eq. (28) is of applicability.

4. Simulation of wind fields

4.1 Procedure for simulation of multiple-point fluctuating wind speeds

The previous sections provide the basic concept and principals for modeling of phase delay spectrum. The model, in fact, is pertinently suitable for the simulation of wide wind fields. The numerical procedure is detailed as follows: (i) define a datum mark and conduct its evolutionary phase spectrum by virtue of the numerical scheme associated with starting-time of phase evolution T_e that we proposed previously (Li *et al*. 2013); (ii) select the appropriate magnification coefficient of phase delay β_y and β_z by fitting the results of model and measured data, the phase delay spectrum of wind speeds at spatial points, relevant to the datum mark, is then generated using Eqs. (19) and (28); (iii) integrate the phase spectrum of the datum mark and the phase delay spectrum to obtain the Fourier phase spectrum of wind speeds at spatial points whereby the time history of fluctuating wind speeds can be readily achieved in conjunction with the Fourier amplitude spectrum using the inverse Fourier transform (Inv-FFT). The flowchart of the numerical procedure is shown in Fig. 10.

4.2 Comparative studies between simulated and measured spatial wind fields

Using the numerical procedure detailed in the previous section, we investigate the sample behaviors of simulated and measured spatial wind fields. The height 10 m at platform point P_1 is served as the datum mark. The vertical wind field is constructed at the four typical heights of P_1, i.e., 10 m, 20 m, 28 m and 43 m. The horizontal wind field is constructed at the height 20 m of the four platform points, i.e., P_1, P_2, P_3 and P_4. The magnification coefficients of phase delay spectrum for horizontal and vertical wind fields are defined as $\beta_y = 35$, $\beta_z = 80$, respectively. The simulated time histories of fluctuating wind speeds in wind fields are shown in Fig. 11. It is seen that the simulated wind speed time series numerically very close to the measured ones.

Besides, the cross-spectral density of simulated and measured fluctuating wind speeds at four typical heights of the platform points is caculated using Eq. (6). It is seen in Fig. 12 that the cross-spectral density of simulated fluctuating wind speeds at typical heights matches well with that of the measured fluctuating wind speeds, indicating that the coherence behaviors of the re-built wind field conform with that of the original wind field.
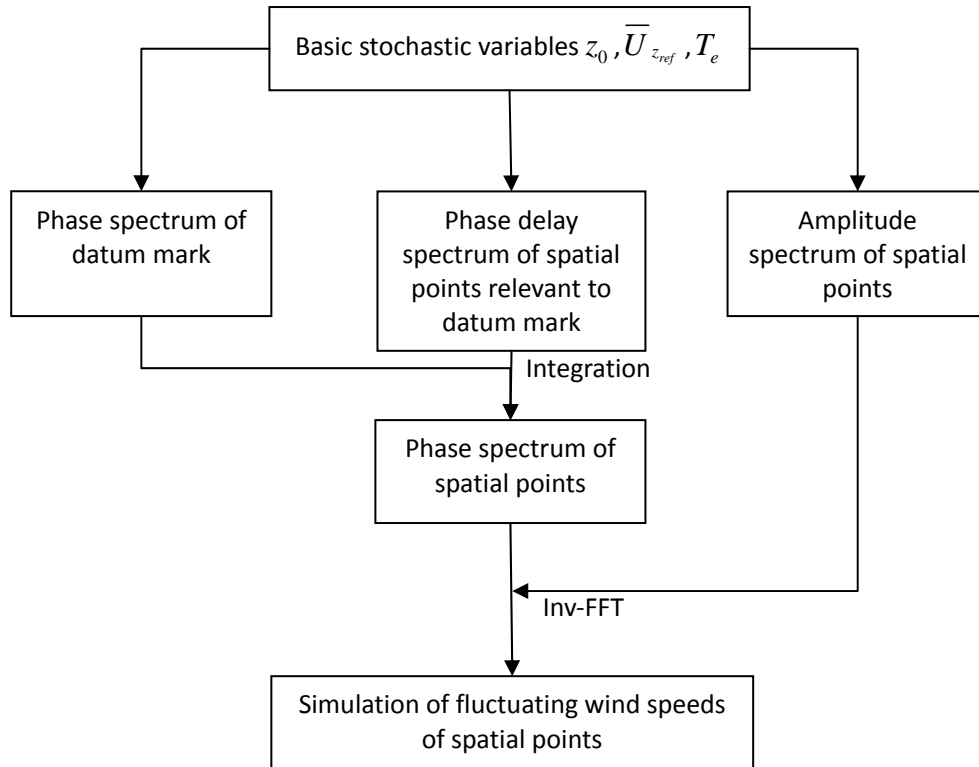
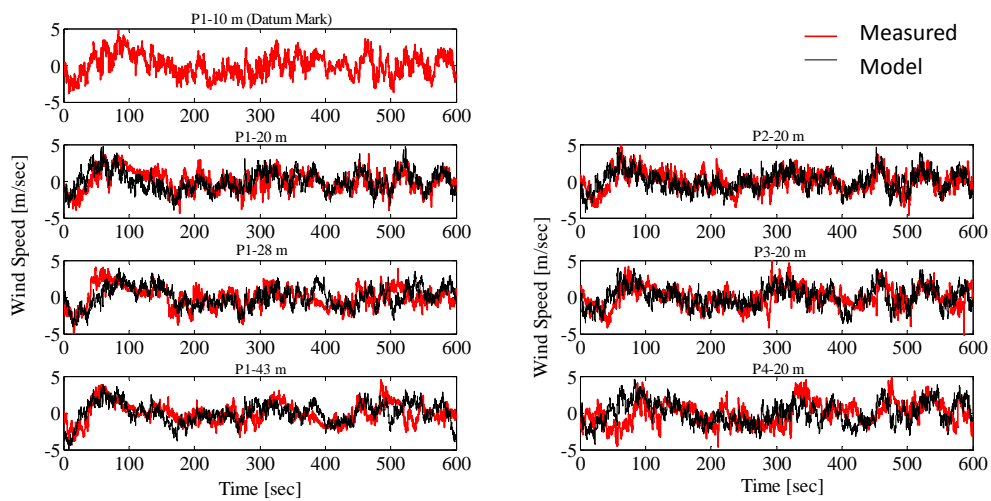Fig. 10 Flowchart of simulation of spatial wind fields

Fig. 11 Simulated and measured time histories of fluctuating wind speeds at typical spatial points of wind fields
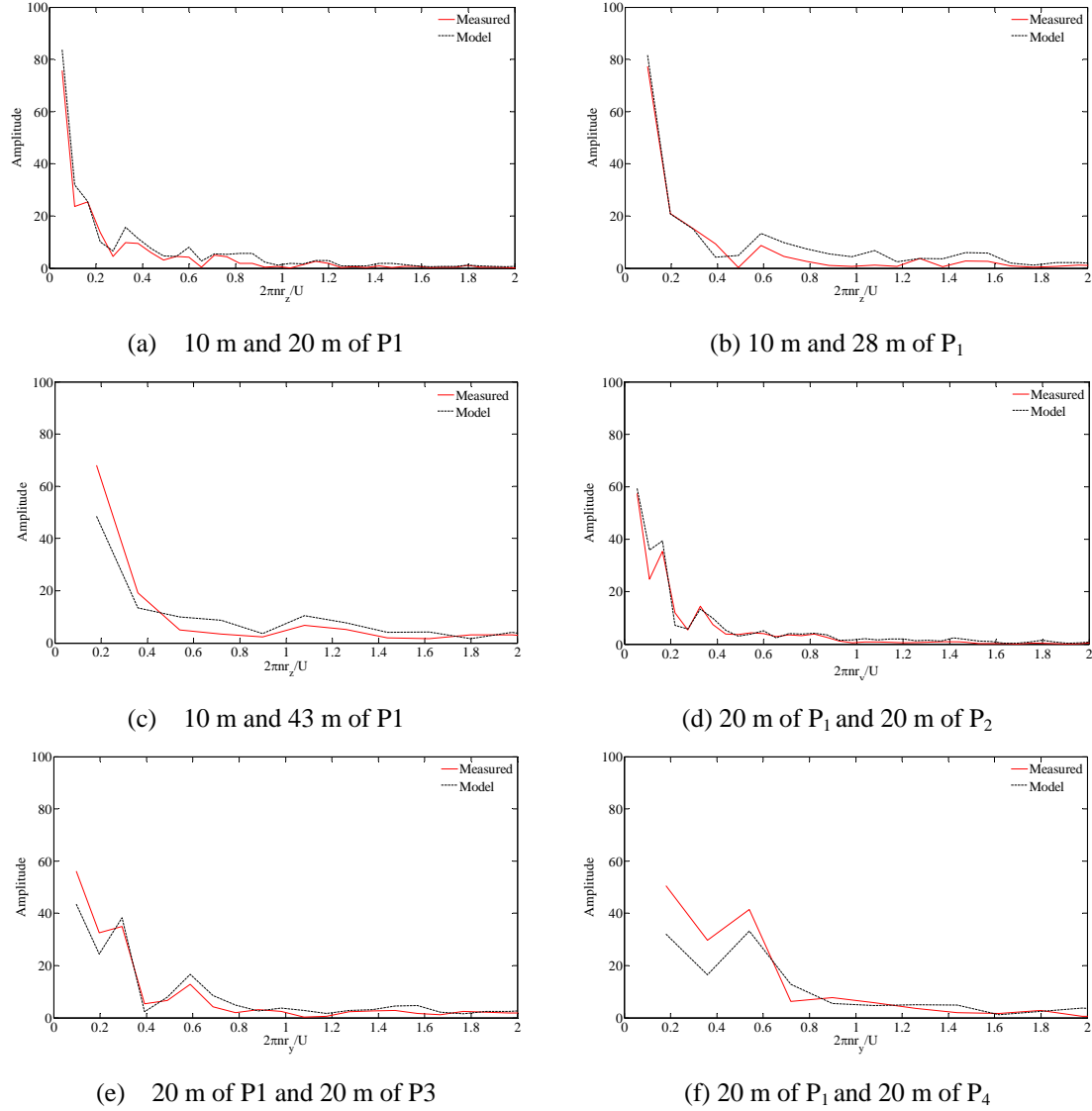
(a)   10 m and 20 m of P1

(b) 10 m and 28 m of P_1

(c)   10 m and 43 m of P1

(d) 20 m of P_1 and 20 m of P_2

(e)   20 m of P1 and 20 m of P3

(f) 20 m of P_1 and 20 m of P_4

Fig. 12 Cross-spectral density of simulated and measured fluctuating wind speeds at four typical heights of the platform points

5. Discussions on spectral representation methods

The spectral representation method is a well-visited numerical simulation scheme. It has been developed into a comprehensive method allowing for simulation of multi-dimensional, multi-variable and non-stationary random processes since it originated in 1954 (Rice 1954). The spectral representation method is widely used in the simulation of wind fields (Shinozuka and Deodatis 1997, Liu *et al.* 2004, Ding *et al.* 2006, Zheng *et al.* 2007, Kareem 2008, Hu *et al.* 2010,

Aung *et al*. 2012, Ye *et al*. 2012). Its essential is to carry out the simulation of the random process matching with objective power spectrum using the superposition technique of harmonic waves with random phases. Fig. 13 shows the flowchart of simulation of spatial wind fields using the spectral representation method.

It is noted that the spectral representation method, at least, underlies the challenges as shown as the following points:

(i) The spectral representation method belongs to the simulation scheme of statistics in essence. In case of the simulation of random processes, the amplitude of harmonic waves relies upon the spectral density. The simulation results, meanwhile, of the objective random process is assessed through the validation of the simulated and the original power spectrum. The spectral density, however, is essentially the statistical characteristics whereby the simulated random process does not include the probabilistic information with statistical moments more than second order.

(ii) The spectral representation method limits in sample selection repeatedly. Since the power spectrum belongs to the ensemble characteristics, the simulated random process cannot feature the sample resurgence of random processes in the real world.

(iii) The initial phases used in the spectral representation method are typically independent stochastic variables distributed in the frequency domain $[0, 2\pi)$ with uniform distribution. This treatment results in a dramatically number increasing of stochastic variables used in the numerical simulation of fluctuating wind-speed fields. The number of the stochastic variables is usually 400-600.

(iv) The essential relationship between the frequency phases, the frequency phase and energy is not included. The result with consequence of these challenges is evident that the numerical simulation of fluctuating wind speeds for stochastic dynamic analysis of structures using the spectral representation method is not only computationally time-consuming but also limited in statistical solution rather than probability density function of responses. The probabilistic solution relevant to statistical moments thus results in the difficulties of accurate assessment of structural reliability.

While the simulation scheme developed in the present paper has a couple of significant benefits over the spectral representation method, as detailed as follows:

(i) The stochastic Fourier spectrum is essentially a stochastic function. Its values hinge on the physical relationship among the basic random variables. It thus exhibits the capacity of re-building up the samples of random processes. In other words, the mapping between the simulated fluctuating wind speeds and the basic random variables is unique and self-consistency.

(ii) The relationship between fluctuating wind speeds at the spatial points in wind fields is governed by the phase delay spectrum. This treatment prompts a ready and succinct scheme for the simulation of fluctuating wind speeds.

(iii) The fluctuating wind speeds is directly generated using the inverse Fourier transform. It bypasses the possible numerical errors due to simulation techniques.

(iv) The random variables involved in Fourier amplitude spectrum and phase spectrum are just the ground roughness length and the mean wind speed, and the evolutionary phase spectrum includes only one random variable T_e as well. It is thus indicated that using only three random variables one could completely simulate a spatial wind field. The reduction of the relevant random variables to the fluctuating wind speed provides a new perspective to the accurate assessment of dynamic reliability of wind-induced structures.
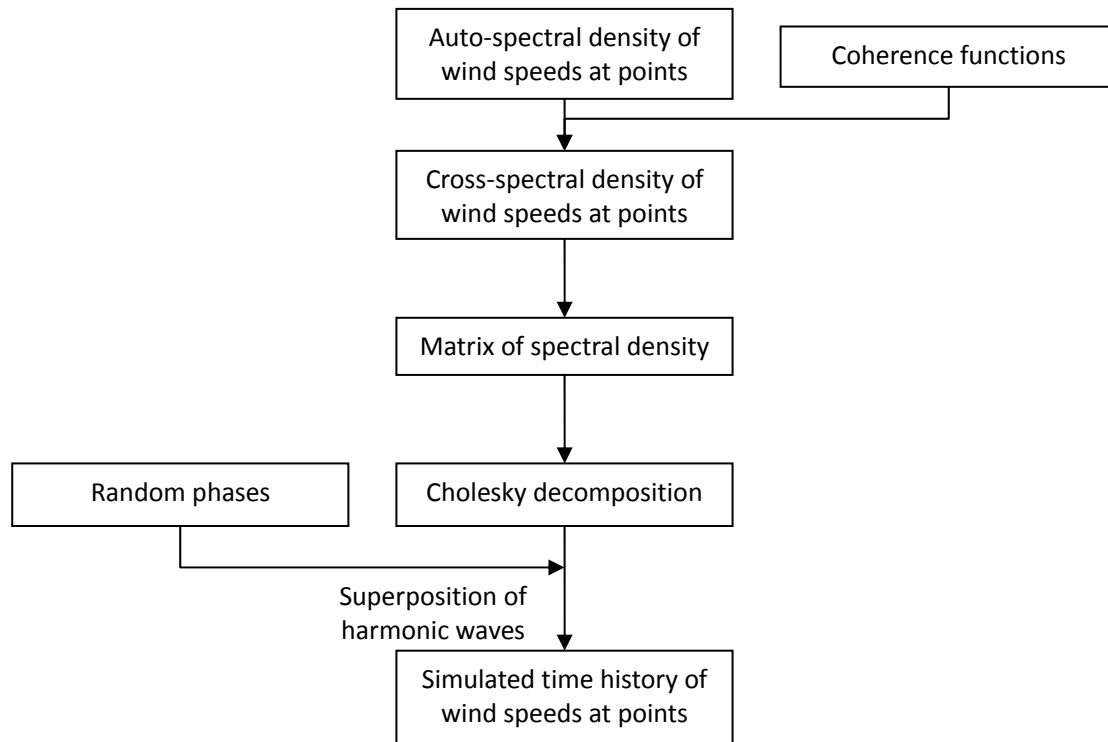
Auto-spectral density of wind speeds at points

Coherence functions

Cross-spectral density of wind speeds at points

Matrix of spectral density

Random phases

Cholesky decomposition

Superposition of harmonic waves

Simulated time history of wind speeds at points

Fig. 13 Flowchart of simulation of spatial wind fields using the spectral representation method

6. Conclusions

The phase delay spectrum is usually used to describe the essential factors of similarities and differences between the time histories of fluctuating wind speeds at two spatial points. In the present paper, we propose a novel model of phase delay spectrum. The model is proved to be of rationality and of applicability using the measured data at spatial points of wind fields. It is indicated in our investigations that the phase spectrum of fluctuating wind speeds at spatial points derives from the integration of phase delay spectrum with the phase spectrum at datum mark defined. The numerical scheme associated with the starting-time of phase evolution provides a new perspective towards the simulation of phase spectrum. The time history of fluctuating wind speeds can readily simulated in conjunction with the stochastic Fourier amplitude spectrum.

Acknowledgements

References

Aung, N.N., Ye, J.H. and Masters, F.J. (2012), "Simulation of multivariate non-Gaussian wind pressure on spherical latticed structures", *Wind Struct.*, **15**(3), 223-245.

Chen, J.J. (1994), "Analysis of engineering structures response to random wind excitation", *Comput. Struct.*, **51**(6), 687-693.

Collins, R., Basu, B. and Broderick, B.M. (2008), "Bang-bang and semiactive control with variable stiffness TM ds", *J. Struct. Eng. - ASCE*, **134**(2), 310-317.

Davenport, A.G. (1961), "The spectrum of horizontal gustiness near the ground in high winds", *Q. J. Roy. Meteor. Soc.*, **87**, 194-211.

Davenport, A.G. (1967), "Gust loading factors", *J. Struct. Division - ASCE*, **93**, 11-34.

Ding, Q.S., Zhu, L.D. and Xiang, H.F. (2006), "Simulation of stationary Gaussian stochastic wind velocity field", *Wind Struct.*, **9**(3), 231-243.

Dyrbye, C. and Hansen, S.O. (1997), *Wind Loads on Structures*, John Wiley & Sons, New York.

Harris, R.I. (1971), "The nature of wind", In *The Modern Design of Wind-Sensitive Structures*, Construction Industry Research and Information Association, London.

Hu, L., Li, L. and Gu M. (2010), "Error assessment for spectral representation method in wind velocity field simulation", *J. Eng. Mech. - ASCE*, **136**(9), 1090-1104.

Kareem, A. (2008), "Numerical simulation of wind effects: A probabilistic perspective", *J. Wind Eng. Ind. Aerod.*, **96**, 1472-1497.

Kristensen, L., Panofsky, H.A. and Smith, S.D. (1981), "Lateral coherence of longitudinal wind components in strong winds", *Bound-Lay. Meteorol*, **21**, 199-205.

Li, J., Yan, Q. and Chen, J.B. (2012), "Stochastic modeling of engineering dynamic excitations for stochastic dynamics of structures", *Probab. Eng. Mech.*, **27**(1), 19-28.

Li, J., Peng, Y.B. and Yan, Q. (2013), "Modeling and simulation of fluctuating wind speeds using evolutionary phase spectrum", *Probab. Eng. Mech.*, **32**, 48-55.

Liu, G., Xu, Y.L. and Zhu, L.D. (2004), "Time domain buffeting analysis of long suspension bridges under skew winds", *Wind Struct.*, **7**(6), 421-447.

Maeda, J. and Makino, M. (1980), "Classification of customary proposed equations related to the component of the mean wind direction in the structure of atmospheric turbulence and these fundamental properties", *T. Architect. Inst.*, **287**, 77.

Panofsky, H.A. and McCormick, R.A. (1954), "Properties of spectra of atmospheric turbulence at 100 metres", *Q. J. Roy. Meteorol. Soc.*, **80**, 546-564.

Panofsky, H.A. and Singer, I.A. (1965), "Vertical structure of turbulence", *Q. J. Roy. Meteorol. Soc.*, **91**, 339-344.

Paroka, D. and Umeda, N. (2006), "Capsizing probability prediction for a large passenger ship in irregular beam wind and waves: Comparison of analytical and numerical methods", *J. Ship Res.*, **50**(4), 371-377.

Rice, S.O. (1954), "Mathematical analysis of random noise", In *Selected Papers on Noise and Stochastic Processes,* edited by N. Wax. Dover, 133-294.

Saranyasoontorn, K., Manuel, L. and Veers, P.S. (2004), "A comparison of standard coherence models for inflow turbulence with estimates from field measurements", *J. Solar Energy Eng. T. - ASME*, **126**(4), 1069-1082.

Schlez, W. and Infield, D. (1998), "Horizonal, two point coherence for separations greater than measurement height", *Bound-Lay. Meteorol.*, **87**(3), 459-480.

Seong, S.H. and Peterka, J.A. (2001), "Experiments on Fourier phases for synthesis of non-Gaussian spikes in turbulence time series", *J. Wind Eng.Ind. Aerod.*, **89**, 421-443.

Shinozuka, M. and Deodatis, G. (1997), "Simulation of stochastic processes and fields", *Probab. Eng. Mech.*, **12**(4), 203-207.

Shinozuka, M. and Jan, C.M. (1972), "Digital simulation of random process and its application", *J. Sound Vib.*, **25**(1), 111-128.

Welch, P.D. (1967), "The use of fast Fourier transform for the estimation of power spectra: A method based on time averaging over short, modified periodograms", *IEEE T. Audio Elect.*, AU-15, 17-20.

Ye, J.H., Ding, J.H and Liu, C.Y. (2012), "Numerical simulation of non-Gaussian wind load", *Sci. China-Technol. Sci.*, **55**(1), 1-13.

Ying, Z.G., Ni, Y.Q. and Ko, J.M. (2005), "Semi-active optimal control of linearized systems with multi-degree of freedom and application", *J. Sound Vib.*, **279**(1-2), 373-388.

Zheng, S.X., Liao, H.L. and Li, Y.L. (2007), "Stability of suspension bridge catwalks under a wind load", *Wind Struct.*, **10**(4), 367-382.

CC